Separation Science and Technology
Publication details, including instructions for authors and subscription information:
http://www.informaworld.com/smpp/title~content=t713708471

Visualizing patterns of protein uptake to porous media using confocal scanning laser microscopy

Thomas Linden[a]; Anders Ljunglöf[b]; Lars Hagel[b]; Maria-Regina Kula[a]; Jörg Thömmes[a]
[a] Institut für Enzymtechnologie, Heinrich-Heine Universität, Düsseldorf, Germany [b] Amersham Pharmacia Biotech, Björkgatan 30, Sweden

Online publication date: 25 April 2002

To cite this Article Linden, Thomas , Ljunglöf, Anders , Hagel, Lars , Kula, Maria-Regina and Thömmes, Jörg(2002) 'Visualizing patterns of protein uptake to porous media using confocal scanning laser microscopy', Separation Science and Technology, 37: 1, 1 — 32
To link to this Article: DOI: 10.1081/SS-120000319
URL: http://dx.doi.org/10.1081/SS-120000319

SEPARATION SCIENCE AND TECHNOLOGY, 37(1), 1–32 (2002)

VISUALIZING PATTERNS OF PROTEIN UPTAKE TO POROUS MEDIA USING CONFOCAL SCANNING LASER MICROSCOPY

Thomas Linden,[1] Anders Ljunglöf,[2] Lars Hagel,[2] Maria-Regina Kula,[1] and Jörg Thömmes[1,*]

[1]Institut für Enzymtechnologie, Heinrich-Heine Universität Düsseldorf, 52426 Jülich, Germany
[2]Amersham Pharmacia Biotech, Björkgatan 30, 751 84 Uppsala, Sweden

ABSTRACT

Confocal scanning laser microscopy has been used to visualize the uptake of fluorescence-labeled proteins to porous stationary phases in finite bath adsorption experiments. Reference proteins were labeled with three different fluorescent dyes and a porous cation exchanger was sequentially incubated with solutions of these protein–dye conjugates. This sequential incubation experiment was used to investigate the pattern of protein uptake during adsorption. The confocal images obtained during the experiments clearly visualized that under certain conditions the adsorbent particles are gradually saturated from the rim to the core, a pattern consistent with the shrinking core model. Changes in the mobile phase conditions (ionic strength, pH) can lead to significant shifts in the uptake pattern, i.e., the further transport of

*Corresponding author.

initially bound molecules to the core, thus making binding sites at the rim available for adsorption of new molecules. At low pH and ionic strength BSA showed an uptake pattern, which was completely in accordance with the shrinking core model, but a clear deviation from this profile was observed at increased ionic strength. During adsorption of a monoclonal antibody a change in pH was sufficient to change the uptake pattern in finite bath adsorption completely. An attempt was made to correlate this behavior to the shape of the equilibrium-binding isotherm. The technique presented here allows unique insights into the details of protein adsorption to porous media and will provide a valuable extension of the existing experimental methods for studies of mechanistic aspects of protein chromatography.

INTRODUCTION

Adsorption chromatography using porous stationary phases is a widely employed unit operation in the preparative separation of proteins. Modeling and simulation are important tools for designing such processes at the technical scale and for optimizing the performance of the separation. In order to perform meaningful simulations experimental methods are required that allow a reliable determination of the model parameters. The kinetics of protein adsorption to porous media may be limited by a number of steps. It is widely accepted, however, that transport within the pore network is the most important factor, which therefore has to be characterized with particular care. Traditionally, finite bath, pulse response, or breakthrough experiments are performed in order to measure the kinetics of protein adsorption. A solution of the target protein is in contact with the stationary phase while the fluid phase protein concentration is monitored as a function of contact time. From the change in fluid phase concentration conclusions are drawn on the penetration of the stationary phase by assuming that all molecules vanishing from the fluid are bound to the stationary phase automatically. A direct measurement of the particle side protein concentration is not possible with these methods. In addition, the particle side protein distribution, which is a central part of all modeling approaches, is not measured.

Alternative techniques attempt to visualize directly adsorbate molecules within a porous stationary phase. Among them are microscopic methods using the fluorescence recovery after photobleaching (FRAP) method, which allows the observation of self-diffusion (without a concentration gradient as driving force) of fluorescence labeled proteins within particles (1). Mattisson used holographic laser interferometry as a method for measuring protein diffusion with gradients imposed in porous agarose gels (2). This technique yields protein profiles within the gel,

Marcel Dekker, Inc.
270 Madison Avenue, New York, New York 10016

which can be used to verify models of intra-particle transport and for determination of diffusion coefficients. It is restricted to situations where a pure protein is observed in a buffered solution and where the porous gel is cast into a diffusion cell. Recently, Lewus and Carta have described an experimental set-up, where the diffusion of cytochrome C in capillaries filled with charged polyacrylamide gels could be visualized and analyzed (3). An experimental method, based on confocal scanning laser microscopy, which is able to visualize multi-component transport phenomena in spherical porous adsorbents, has been developed in our laboratories. Porous adsorbents are incubated with proteins labeled by a fluorescent dye in a finite bath experiment. Single adsorbent particles are removed from the experiment and are observed by confocal microscopy. Laser light is focused on a defined spot within the adsorbent particle and is used to excite fluorescence at the focal point. A pinhole aperture arrangement allows the specific registration of fluorescence emitted from the focal plane, while out-of focus light is effectively blocked from the detector. A scanning procedure allows the determination of the distribution of local fluorescence intensity—which can be related to protein concentration—across the particle diameter, thus yielding the distribution of adsorbed protein molecules (4). Figure 1 shows a simplified picture of the beam paths in a confocal microscope and the experimental results, which can be obtained with this set-up. By using this protocol for the analysis of single component protein uptake in finite bath experiments, it was possible for the first time to measure the protein profile within a porous adsorbent as a function of incubation time. The data obtained were evaluated in terms of the fractional approach to equilibrium, which corresponded well with data calculated from the decrease in protein concentration in the fluid phase (5). Because confocal microscopes can be equipped with several independent detection systems, the simultaneous penetration of porous media by two or more proteins can be observed in situ by coupling different fluorescence labels to different proteins. This was realized successfully with the example of the separation of BSA and human IgG on cation exchange and affinity media (6) and yielded elucidating images that demonstrated how the distribution of proteins can be dominated by displacement effects.

The unique potential of the confocal method for visualizing internal transport phenomena has encouraged us to investigate the patterns of protein uptake to porous adsorbents in greater detail. An interesting question in protein adsorption is, whether a protein, which has been bound to a particular ligand on the internal adsorbent surface, will remain immobilized at this specific location or whether it is able to move on towards the interiors of the particle, thus making room for binding of other protein molecules. In order to assess this question, we have made use of the possibility to work with several fluorescent dyes at the same time in our confocal set-up. After choosing three dyes, which have a suitable spectral behavior in a way that they are independently detectable by the microscope, samples of one protein were labeled with these dyes and the uptake

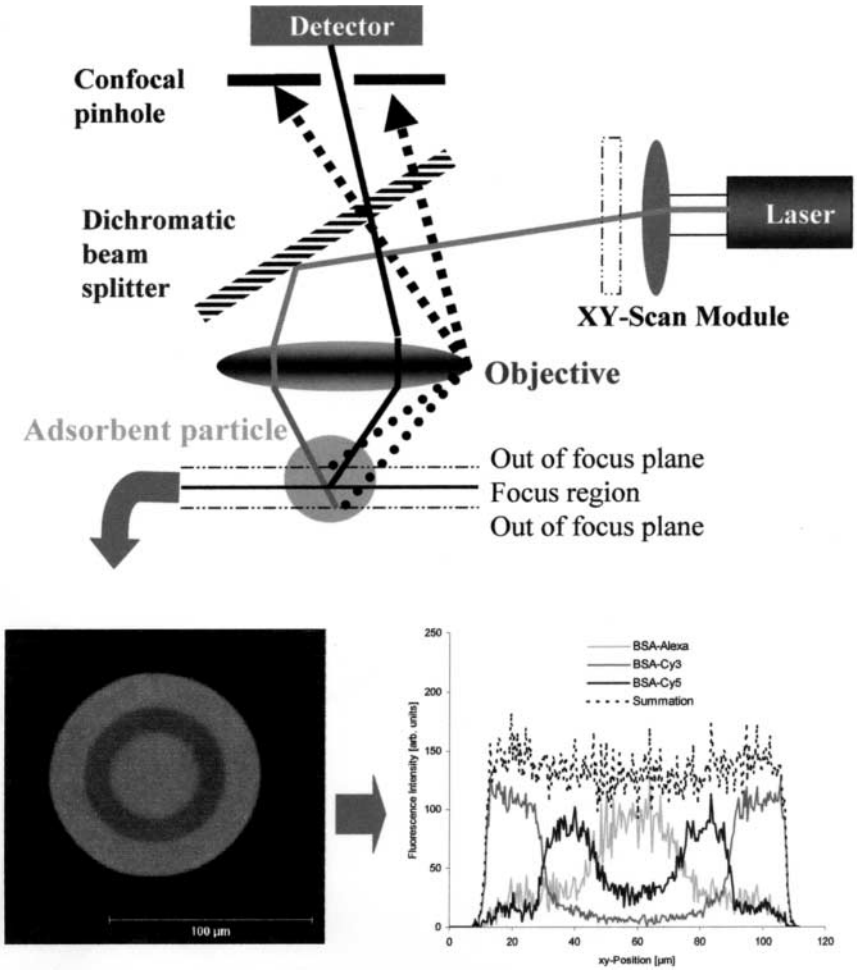

Figure 1. Confocal principle and evaluation the confocal images.

of the protein to a porous stationary phase was investigated in finite bath experiments. Microscopic observation of single adsorbent beads with the confocal technique allowed the measurement of the distribution profile of the protein as a function of residence time in the finite bath. The three batches of differently labeled protein were consecutively incubated with the same batch of a suitable stationary phase. The rationale behind this experiment was as follows: incubating a solution of the target protein labeled with dye #1 for a short period of time will permit a certain degree of penetration of the protein into the adsorbent.

This penetration will be visible in the confocal image as a narrow ring of protein with the rest of the particle not yet being occupied. Incubation of this pre-loaded particle with a solution of the same protein labeled with dye #2 for another short period will show, whether this ring of protein stays in place. This would force the freshly penetrating "second" set of proteins to move further into the porous adsorbent, thus forming a second ring of protein, which can be distinguished from the first one by its differing fluorescence excitation and emission properties. Then, if the same batch of adsorbent, which is now pre-loaded with two rings of the same protein, is equilibrated with the same protein labeled with dye #3, the rest of the adsorbent particle will be filled up with a core of protein, which can be differentiated again in the confocal image by its fluorescent properties. In the equilibrium situation therefore, a target type of confocal image with three clearly separate and differently colored rings should be expected, when this experiment is performed with a protein, which under the experimental conditions chosen stays in its position after it has been bound once to a certain region of the internal surface. Conditions allowing for a "movement" of the bound protein (irrespective of the putative mechanism causing this movement) will result in a distorted confocal image. In this case the first ring of protein will spread out during incubation with the second set of labeled protein, and after incubation with the third protein–dye combination the target type of image should show diffuse boundaries between the rings. Depending on the "mobility" of the bound protein a situation may arise, where the three fluorescent dyes in equilibrium are distributed evenly over the particle diameter. These experiments will give valuable insight into the processes occurring during adsorption of proteins to porous media, as well as the equilibrium distribution of proteins as a function of fluid phase conditions. They may also serve as a basis for discussions on potential mechanisms of internal protein transport, which are found frequently in literature. Many authors have discussed that, besides protein transport in the pore fluid, surface diffusion of bound proteins may contribute to the overall influx into porous media (3,7–11). Experimental evidence for this contribution is hard to obtain solely from fluid phase data; the technique presented here may help to widen the data base available for interpretation.

In the experimental procedure it was important to account for potential influences of the fact that we are working with labeled proteins and to ensure that the adsorbent was exposed to a protein solution of unchanged concentration during exchange of dye–protein conjugates. Therefore, the experiment was performed simultaneously with three batches of adsorbents, where each protein dye combination was incubated with one batch of stationary phase for a defined period of time and where the respective supernatants were transferred to a batch of adsorbent, which was in contact with a different protein–dye conjugate before. The experimental procedure and the appending pipetting scheme is shown in Fig. 2.

MARCEL DEKKER, INC.
270 Madison Avenue, New York, New York 10016

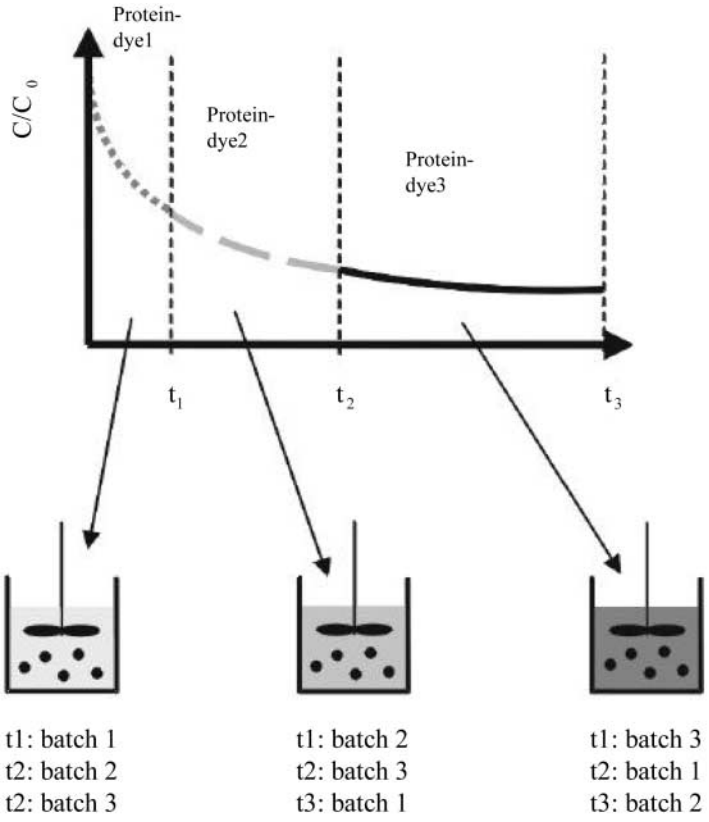

Figure 2. Principle of the three-conjugate adsorption experiments.

Ion exchange adsorption chromatography is used in almost every industrial protein purification process, thus the investigations outlined here were performed to study this particular mechanism. As the behavior of proteins in these experiments can be correlated to the nature of the adsorption equilibrium (besides mechanistic speculations), measurements were conducted at varying pH and conductivity—parameters that are well known to influence the equilibrium. In order to correlate the phenomena observed to the nature of the equilibrium, adsorption isotherms were determined for all experimental conditions.

When experiments are performed with fluorescence modified proteins, it is of utmost importance to ensure that neither equilibrium nor kinetics of the adsorption are influenced by the coupling of the fluorescent dye. Therefore, the labeled proteins had to be compared on the basis of their isoelectric point,

molecular weight, and chromatographic behavior in cation exchange. Subsequently, the dependence of protein uptake pattern on the fluid phase conditions will be discussed in the example of adsorption of bovine serum albumin (BSA) and a monoclonal antibody (IgG2a, mIgG) to the cation exchange SP Sepharose^{TM} FF (Amersham Pharmacia Biotech, Uppsala, Sweden).

MATERIALS AND METHODS

Proteins

BSA Fraction V (66430 g/mol, pI = 4.8) with purity greater than 98% was obtained from Sigma Aldrich (Deisenhofen, Germany). Monoclonal IgG2A antibody (mIgG) was purified from hybridoma culture supernatant in our laboratories to purity greater than 99%. The molecular weight of the antibody was 147645 g/mol measured by mass spectroscopy and the isoelectric point was determined to be approximately 6.0 (data not shown).

Adsorbents and Chemicals

SP Sepharose FF (particle radius, $r_p = (3\text{–}7.5) \times 10^{-5}$ m) was obtained from Amersham Pharmacia Biotech (Uppsala, Sweden). A sieved fraction of SP Sepharose FF ($r_p = (4.5\text{–}5.5) \times 10^{-5}$ m) was used in all confocal experiments. All other chemicals were of analytical grade and were ordered from commercial sources. Cy5 and Cy3 reactive dye were obtained from Amersham Pharmacia Biotech (Uppsala, Sweden) and Alexa 488^{TM}, a FITC derivative, from Molecular Probes (Leiden, The Netherlands). The coupling of the protein with the fluorescent dyes was performed according to the standard procedures recommended by the manufacturers.

Characterization of the Protein–Dye Conjugates

High Pressure Liquid Chromatography Analysis

Small samples (0.02 mL, 2 mg/mL) of unlabeled protein and protein–dye conjugates were analyzed with a Shimadzu HPLC 10ADvp system (Duisburg, Germany) with a flow rate of 0.5 mL/min. After loading the samples on a Sepharose FF column (vol. 1 mL) equilibrated with 50 m*M* acetate buffer pH 5.0 the samples were eluted in a linear salt gradient of 20 column volumes up to 50 m*M* acetate buffer supplemented with 1 *M* NaCl.

MARCEL DEKKER, INC.
270 Madison Avenue, New York, New York 10016

The elution was monitored by detecting the absorbance at 220 nm with the UV/VIS SPD10Avp Detector (Shimadzu, Duisburg, Germany). As a characteristic value the average of three retention times per unlabeled protein and protein–dye conjugate was used to investigate and quantify the deviations between retention of the different molecular species.

Gel Filtration Experiments

Gel filtration experiments were performed on Superdex^{TM} 200 (Amersham Pharmacia Biotech, Uppsala, Sweden) equilibrated with 50 m*M* potassium phosphate buffer pH 6.5 and supplemented with 150 m*M* KCl using an automated FPLC^{TM} system (2 × P500 Pump, LCC-501 Controller) from Amersham Pharmacia Biotech (Uppsala, Sweden). The elution of unlabeled protein and protein–dye conjugate samples (1 mL, 2 mg/mL) was determined at a fluid flow of 1 mL/min and monitored by detecting the absorbance at 280 nm. The distribution coefficient, K_{av} was calculated and the average of two values per sample was used for both proteins and their labeled species.

Isoelectric Focusing

The isoelectric points of proteins and conjugates were determined by isoelectric focusing on a 1% agarose focusing gel with the pH range 3–7 according to standard protocols.

Multi Color Analysis of Protein Adsorption

Instrumentation

The confocal images were generated using a Leica TCS SP confocal laser scanning microscope (Heidelberg, Germany) supplied with an argon/krypton laser. A VersaFluor fluorometer from Bio Rad Laboratories (CA, USA) was used with a filter set of (Exc. 496 nm; Em. 520 nm) for the Alexa and (Exc. 650 nm; Em. 670 nm) for the Cy5 conjugates for determination of the concentration in the fluid phase. The Cy3 conjugate samples were analyzed with a fluorescence spectrometer LS 50B from Perkin Elmer (Norwalk, USA) with the monochromator set-up (Exc. 550 nm and Em. 570 nm).

The confocal images were evaluated with the supplemented TCS SP Software based on Microsoft Excel.

Finite Bath Experiments

Four 2-mL tubes were each filled with 1.5 mL of protein solution consisting of a 1:10 ratio of labeled protein conjugate and the unlabeled species. The total initial protein concentration was equal in all batches (approximately 2.5 mg/mL). The finite bath experiment was started by adding a defined volume of a 1:3 (w/w) SP Sepharose FF slurry. The tubes were incubated for a defined time in an overhead-shaker. A 0.007 mL sample of each batch was taken for confocal microscopic analysis.

The batches were centrifuged for 30 sec at 14000g and a sample of 100 μL was collected from the supernatant for the determination of the fluid phase protein concentration. Then the supernatants were exchanged almost quantitatively between three batches including all different protein–dye conjugates (Fig. 2). The fourth batch served as a control experiment and was not involved in this procedure but further incubated without any change in protein solution. The batches were further incubated for a second period of time and the sample collection, analysis, and exchange was repeated once again. The batches were incubated until the adsorption equilibrium was reached and samples of particles and fluid phase were analyzed. The incubation times t were chosen depending on the rate of adsorption kinetics to allow detection of each protein conjugate pulse over the whole experimental time.

Confocal Microscopic Analysis

A confocal laser scanning microscope uses only the fluorescence emission originating from the focal plane for image generation while fluorescent light emitted from out of focus regions is efficiently blocked by a pinhole aperture in front of the detector (Fig. 1). This results in an increased depth resolution and allows optical sectioning of a three dimensional object along different optical axes. The principles and advantages of confocal microscopy have been described extensively in the literature (12).

In order to obtain the correct particle diameter from the image, confocal microscopic analysis was performed by horizontal scanning of the optical xy-plane through the middle of the adsorbent particle sample (Fig. 1). A 63 × NA 1.32 oil immersion objective lens was used for generating confocal images with a size of 512 × 512 pixels. The instrument is able to recalculate these pixels, defined as two dimensional picture elements, into real length in μm.

The argon/krypton laser provided excitation of Alexa as a FITC derivative at 488 nm, Cy3 at 568 nm and Cy5 at 647 nm. The spectral detection settings of the microscope were 515–540 nm for Alexa, 588–620 nm for Cy3 and 670–690 nm for Cy5.

MARCEL DEKKER, INC.
270 Madison Avenue, New York, New York 10016

For an independent detection of all protein–dye conjugates all images were generated using a special sequence scanning procedure recommended by the manufacturer for separate detection of dyes with a small spectral overlap. During this scanning program the Alexa and the Cy5 fluorescence emission (no spectral overlap) were excited and detected simultaneously, prior to a separate Cy3 fluorescence detection without any Alexa and Cy5 settings, so that an influence of energy transfer or cross-talk between different detection channels was effectively removed during the experiments. As each fluorescent dye is coupled to protein molecules with a different molar ratio of dye to protein, a direct comparison of the absolute intensity profiles is not possible. Each conjugate will result in a specific fluorescence response per protein molecule, so a calibration of the spectral signals is required. This was obtained by incubating SP Sepharose FF particles with solutions of three single protein–dye conjugates of identical composition. After equilibrium was obtained, the three fluorescence spectra were overlapped, as it was reasonable to assume that the absolute equilibrium capacity is independent from the fluorescence labeling. Therefore, the adjustment of the three equilibrium spectra to the same level allows direct comparison of all spectra obtained with these specific settings. Figure 3 shows the adjusted spectra of SP-Sepharose FF particles which were incubated with solutions of three individual BSA–dye conjugates (BSA–Alexa, BSA–Cy3, BSA–Cy5).

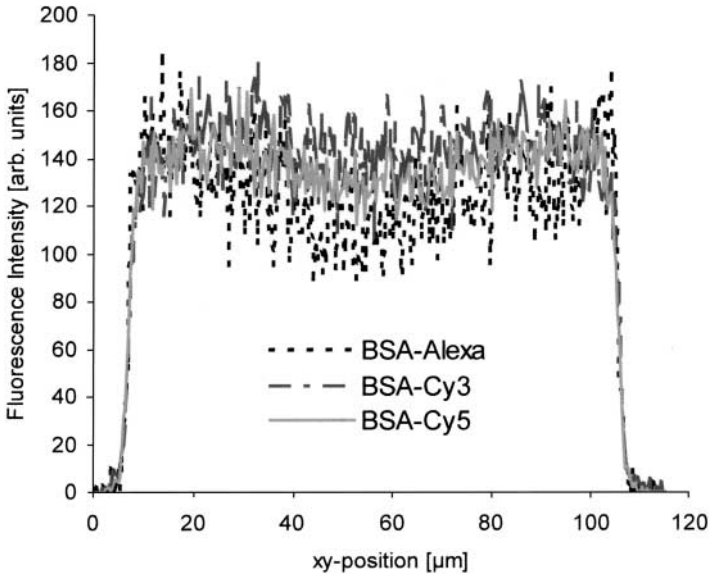

Figure 3. Calibration spectrum BSA 50 m*M* pH 5.0: BSA–Alexa (dotted lines), BSA–Cy3 (dark gray lines), BSA–Cy5 (light gray line).

MARCEL DEKKER, INC.
270 Madison Avenue, New York, New York 10016

Evaluation of the Experimental Data

The sequential scanning technique delivers an image of the fluorescence distribution of up to three different fluorescent molecules in a horizontal section of an adsorbent particle. The three different fluorescence responses were transformed into single images by an overlay procedure. The resulting image is translated into intensity profiles for each labeled species using the microscope's analysis software (see Fig. 1). The fluorescence intensity profile is expressed as the fluorescence intensity in arbitrary units against the xy-position in μm and represents the fluorescence intensity distribution over the particle diameter and this distribution can be related to the local amount of bound protein.

A quantitative evaluation of the profiles was performed as follows: for each fluorescence intensity value I_{rad}, depending on the radial position $(r_a - r_i)$, a shell volume intensity $I^{\text{shell}}_{\text{integr.}}$ was calculated using Eq. (1).

$$I^{\text{shell}}_{\text{integr.}} = \bar{I}_{\text{rad}} \left[(r_a^3 - r_i^3) \frac{4}{3} \pi \right] \tag{1}$$

A summation of all shell volume intensities divided by the particle volume yields the relative capacity $Q^{\text{ch}}_{\text{rel}}(i)$ with $i = 1$–3 for three channels (Eq. (2)).

$$Q^{\text{ch}}_{\text{rel}}(i) = \frac{I_{\text{integr.}}}{V_{\text{p}}} = \frac{\sum_{\text{shells}} (I^{\text{shell}}_{\text{integr.}})}{V_{\text{p}}} \tag{2}$$

A further summation of the relative channel capacities yields the relative capacity Q_{rel}, which represents the relative concentration of the adsorbate in the stationary phase (Eq. (3)).

$$Q_{\text{rel}} = \sum_{i=1}^{3} Q^{\text{ch}}_{\text{rel}}(i) \tag{3}$$

From one experimental series with all possible protein–dye sequences and a single conjugate control, four relative capacities Q_{rel} per time value are obtained, which can be used for calculation of the mean.

The absolute capacities $Q_{\text{abs}}(t)$ were calculated from the fluid phase protein balance using Eq. (4) with the initial and actual concentration of supernatants c_{i} and c_{t}, the fluid volume V_{sys}, and the total particle volume V_{gel}.

$$Q_{\text{abs}}(t) = \frac{V_{\text{sys}}(c_{\text{i}} - c_{\text{t}})}{V_{\text{gel}}} \tag{4}$$

The relative capacity Q_{rel} can be translated to an absolute capacity in mg protein per mL adsorbent by plotting Q_{rel} vs. Q_{abs} in a parity plot.

MARCEL DEKKER, INC.
270 Madison Avenue, New York, New York 10016

Adsorption Isotherms

The adsorption isotherms were generated using a static micro batch method developed by Karol Lacki, Amersham Pharmacia Biotech (Uppsala, Sweden). A small amount (35 μL) of adsorbent particles were equilibrated to saturation with a dilution series of the sample protein (800 μL/well) in a 96 deep well micro plate purchased from Beckmann Instruments GmbH (Munich, Germany).

Constant volumes of adsorbent were generated by using a Microcube 96, a prototype obtained from Amersham Pharmacia Biotech (Uppsala, Sweden). The middle part of this three part sandwich arrangement contains 96 holes with a defined volume of 35 μL. By filling the microcube with a suitable slurry (adsorbent content >50%) and centrifuging for 5 min using a J6 centrifuge with a JR3.2 rotor purchased from Beckmann (Munich, Germany), 96 uniform volumes of 35 μL of packed adsorbent beads were obtained, which were then added to the protein solution batches with a metal pin. The deep well plates were allowed to reach equilibrium and after further centrifugation (same conditions), the concentration of the protein samples was determined by measuring the UV absorbance at 280 nm.

The experimental data were fitted using the Langmuir model with the association equilibrium constant K_a and Q_{max} as characteristic parameters (Eq. (5)).

$$Q = \frac{Q_{max} K_a c_{eq}}{(1 + K_a c_{eq})} \tag{5}$$

RESULTS AND DISCUSSION

Validation of the Approach

As outlined in the introduction, it has to be ensured that covalent coupling of fluorescent dyes to the proteins under investigation does not influence equilibrium and kinetics of their adsorption to the porous stationary phase. Conserved adsorption properties were verified by analyzing the retention of the various protein–dye conjugates in gradient elution from the cation exchanger used. Table 1 summarizes the data obtained. The maximum deviation between the retention time of labeled and unlabeled protein was 3%. Therefore, it can be stated that the adsorption of neither mIgG nor BSA is significantly influenced by the coupling of fluorescent dyes. For further confirmation, analytical gel chromatography experiments were conducted. Molecular size and conformation are the main factors influencing retention in gel filtration. As the size of the

MARCEL DEKKER, INC.
270 Madison Avenue, New York, New York 10016

Table 1. Retention Time of Labeled and Unlabeled Proteins in Cation Exchange Gradient Elution on SP Sepharose FF

Sample	Retention Time (min)	Deviation (%)	K_{av}	Deviation (%)
mIgG Alexa	18.59	0.2	n.d.	n.d.
mIgG Oregon	18.07	3	0.39	6
mIgG Cy3	18.37	1.4	n.d.	n.d.
mIgG Cy5	18.5	0.7	0.38	0.5
mIgG unlabeled	18.63	—	0.38	—
BSA Alexa	13.78	1		
BSA Oregon	14.06	1	0.504	0.8
BSA Cy3	13.68	1.8	n.d.	n.d.
BSA Cy5	13.81	0.9	0.500	—
BSA unlabeled	13.93	—	0.500	—

coupled fluorescent dyes is small compared with the proteins used, the absolute increase in molecular weight by the coupling procedure should be negligible. Therefore, a comparison of the K_{av} values of labeled and unlabeled proteins should indicate whether the labeling has changed the protein conformation. As can be found from Table 1, the maximum deviation in K_{av} was only 6%, which confirms the statement of conserved protein characteristics despite modification with fluorescent dyes. As a final proof the isoelectric points of the different protein dye conjugates were determined. Again, no significant deviations were observed (data not shown), thus ensuring that analysis of the protein uptake pattern in finite bath experiments will not be biased by labeling effects.

Finite Bath Experiments

Thex analysis of adsorption experiments conducted after the scheme shown in Fig. 2 was used to investigate the pattern of BSA and mIgG uptake to SP Sepharose FF particles at different pH values and conductivity. Figure 4* shows confocal images from such an experimental series in the example of BSA adsorption in 50 m*M* acetate buffer at pH 5.0. The first three columns of confocal images show SP Sepharose FF particles, which were consecutively incubated with three BSA–dye conjugates according to Fig. 2, while in the right lane a

*Please see color insert for Fig. 4.

MARCEL DEKKER, INC.
270 Madison Avenue, New York, New York 10016

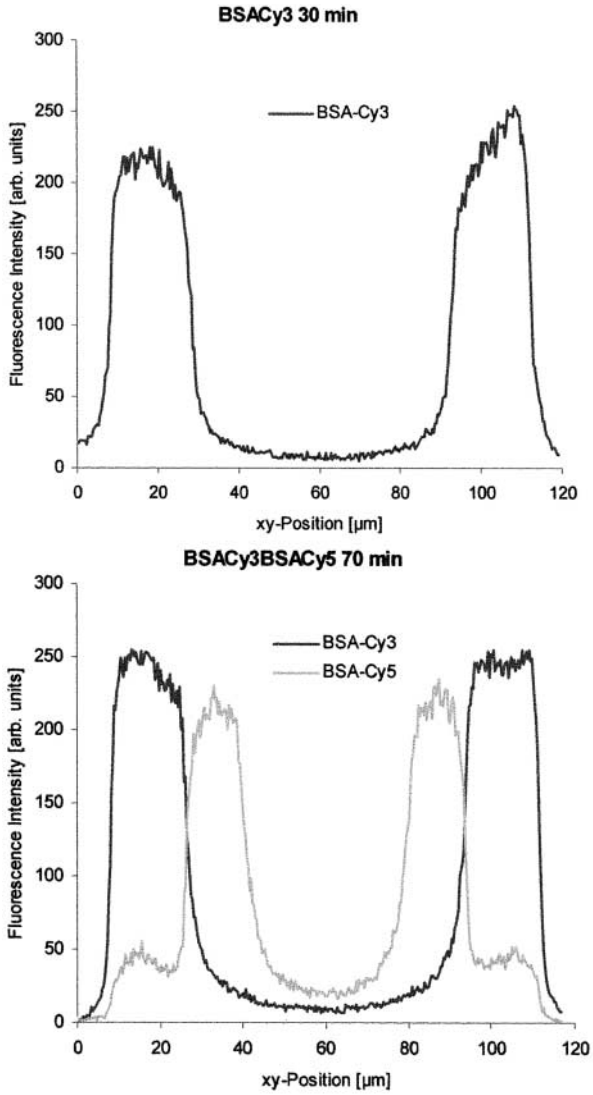

Figure 5. Fluorescence intensity profiles of a sequential incubation of fluorescence labeled BSA at pH 5.0 with SP Sepharose FF; 50 m*M* acetate buffer (0–30 min BSACy3; 30–70 min BSACy5; 70 min −24 hr 10 min BSA–Alexa).

MARCEL DEKKER, INC.
270 Madison Avenue, New York, New York 10016

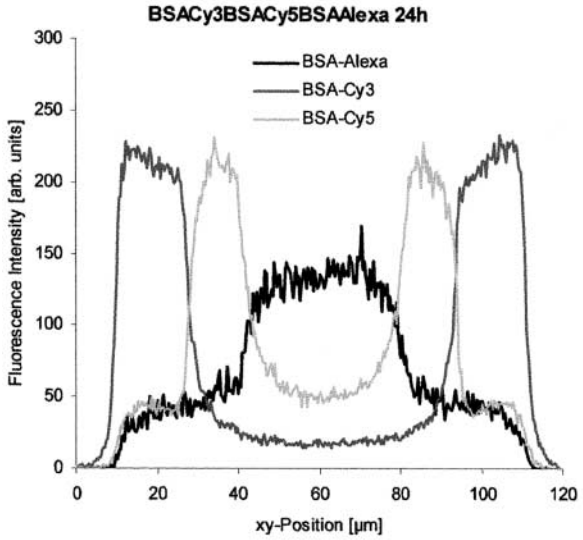

Figure 5. Continued.

control experiment is provided, where only one BSA–dye conjugate had been used. This procedure was executed in all experiments described below, although only one particular sequence of incubation will be shown and discussed in each case. In the example shown in Fig. 4, a sharp colored ring is found in the outer region of the adsorbent particles after 30 min of incubation. This can be attributed to the trivial fact that the protein first binds to the external regions of an unloaded spherical stationary phase. After 70 min and 26 hr of incubation with the subsequent BSA–dye conjugates this initial ring changes neither in position nor in intensity. The second incubation with a different conjugate for another 40 min results in a second ring, which is located further inside the particle adjacent to the first ring. The final incubation with the third BSA–dye conjugate completes the observed ring pattern and yields an image of three distinct rings at equilibrium. The three experiments yield identical patterns, thus demonstrating that the experimental result is independent of the nature and sequence of fluorescence labeled proteins. Furthermore, the progress of protein penetration into the particles matches the pattern in the control experiment. This behavior was found in all experiments discussed later and shows that a generic experimental set-up has been developed. The intensities of the fluorescence signals of the individual protein–dye conjugates can be used to generate the protein concentration profiles over the particle diameter. The corresponding profiles for one sequential series with a first incubation with BSA–Cy3 for 30 min followed by an incubation with BSA–Cy5 (30–70 min) and BSA–Alexa (70 min to 26 hr), which is

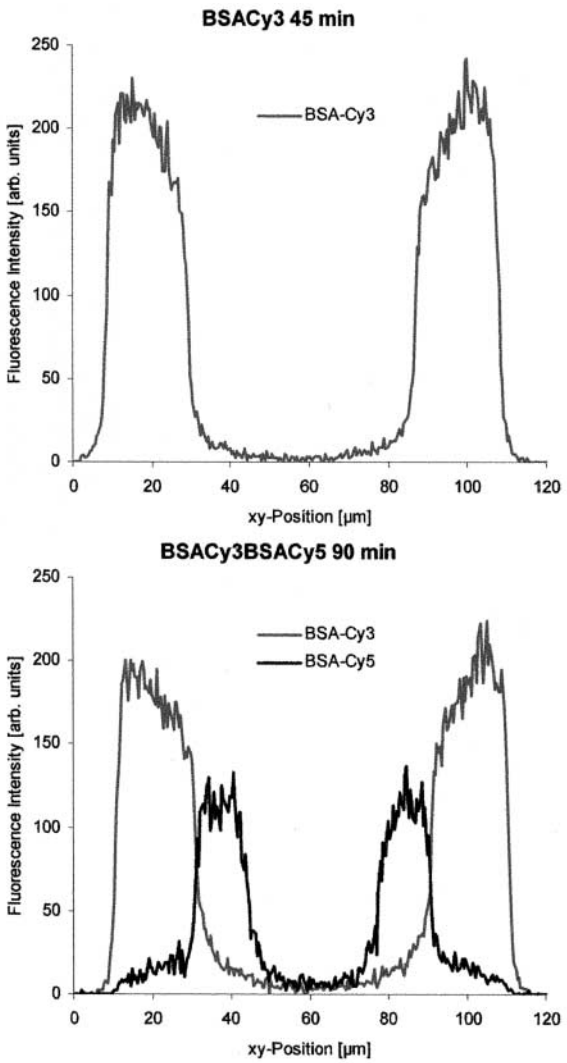

Figure 6. Fluorescence intensity profiles of a sequential incubation of fluorescence labeled BSA at pH 4.5 with SP Sepharose FF; 50 m*M* acetate buffer (0–45 min BSACy3; 45–90 min BSACy5; 90 min–22 hr 30 min BSA–Alexa).

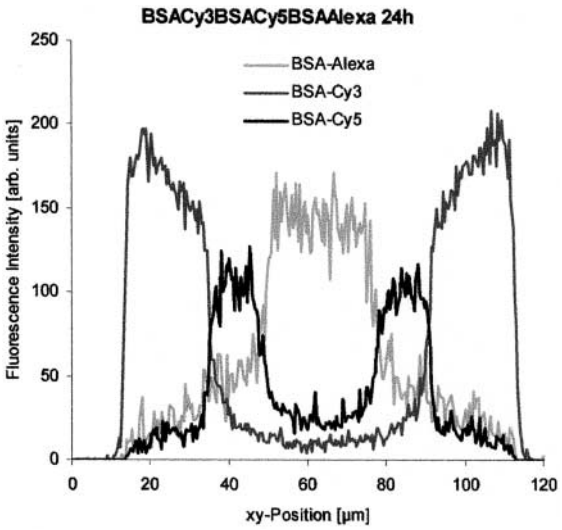

Figure 6. Continued.

shown in the second image column in Fig. 4, are shown in Fig. 5. The ring pattern translates into sharp intensity profiles with the respective signals for the first and second incubation period remaining constant during further incubation, as could be predicted qualitatively from visual inspection of the images in Fig. 4. As the fluorescence response of the individual conjugates represents BSA molecules bound to the stationary phase during the particular incubation step, this result indicates that as soon as BSA is bound to individual cation exchange ligands within the porous adsorbent there is no further movement of the bound molecules under these conditions. The stationary phase is gradually filled up from the outmost ligands to the core with the adsorbate molecules passing already bound species until they find the next available ligand. It is interesting to note that this pattern of protein uptake is accurately described by the so-called shrinking core model, which has been developed for adsorption of gases and small molecules to porous media under conditions characterized by irreversible or very favorable binding equilibrium and pore diffusion as the major mechanism of particle side transport (13). This model has also been used to simulate single protein uptake kinetics in finite bath experiments based on fluid side concentration measurements (11).

When this experiment is conducted at a reduced pH of 4.5, qualitatively the same fluorescence intensity profile pattern is obtained (Fig. 6). The absolute intensity values are certainly different in comparison with the experiment performed at pH 5.0. This can be attributed to the lower pH, which certainly affects the quantum yields of the fluorophores used. Moreover, in this case the

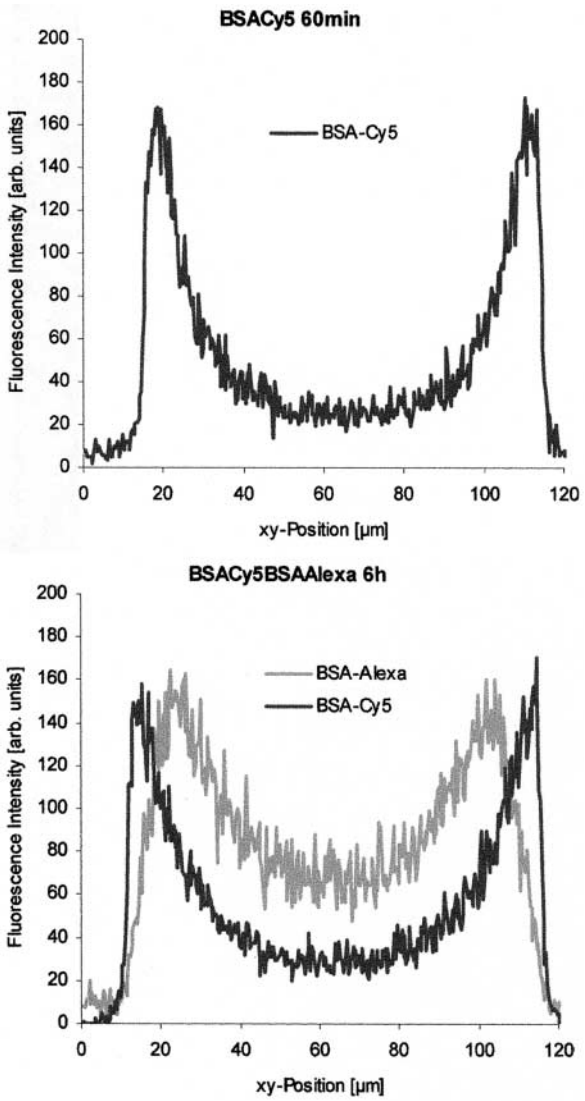

Figure 7. Fluorescence intensity profiles of a finite bath experiment with BSA and SP Sepharose FF at pH 5.0; 150 m*M* acetate buffer (0–60 min BSA Cy5; 60 min–5 hr BSAAlexa; 5–34 hr BSACy3).

MARCEL DEKKER, INC.
270 Madison Avenue, New York, New York 10016

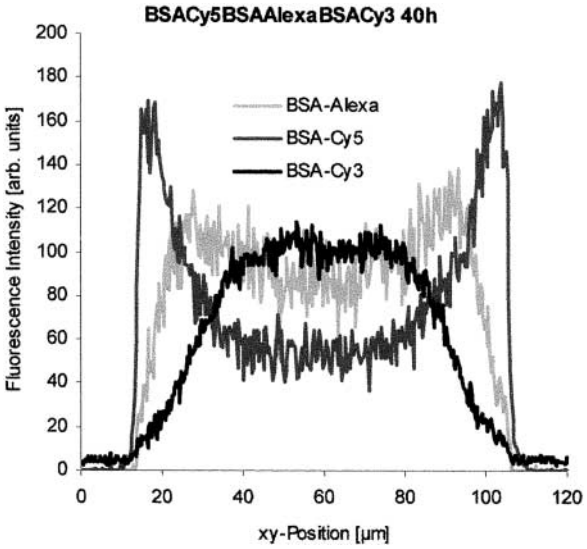

Figure 7. Continued.

BSA molecules do not change their position within the porous adsorbent after binding to the ligands and the particles fill up with protein from the rim to the core of the particle. A further variation of experimental conditions was achieved by increasing the conductivity in the mobile phase. Figure 7 shows fluorescence intensity profiles after sequential incubation of three BSA–dye conjugates in 150 m*M* acetate buffer at pH 5.0. As the adsorption kinetics under these conditions are very slow the incubation times for the individual conjugates had to be extended in order to receive a suitable intensity for each fluorescence signal. The first incubation was performed using a BSA–Cy5 conjugate, whose intensity profile is represented by the dark gray lines. With conductivity in the fluid phase being higher than before the protein profile after the initial incubation period (60 min) is not as sharp and it changes during the second (60 min to 6 hr) and the third (6–40 hr) incubation period where the pre-loaded particle had been incubated with a BSA–Alexa and a BSA–Cy3 conjugate, respectively. This might indicate that once BSA molecules are bound to the ligands they can move further to the core of the particle, thus making room for subsequent incoming molecules, which can bind to the now available ligands at the particle rim. Looking at the profile measured for the second BSA–dye conjugate (BSA–Alexa, light gray line), which had been used in the second incubation period from 60 min to 6 hr, this finding is confirmed. This conjugate seems to move further into the adsorbent during the third incubation period. All three conjugates seem to

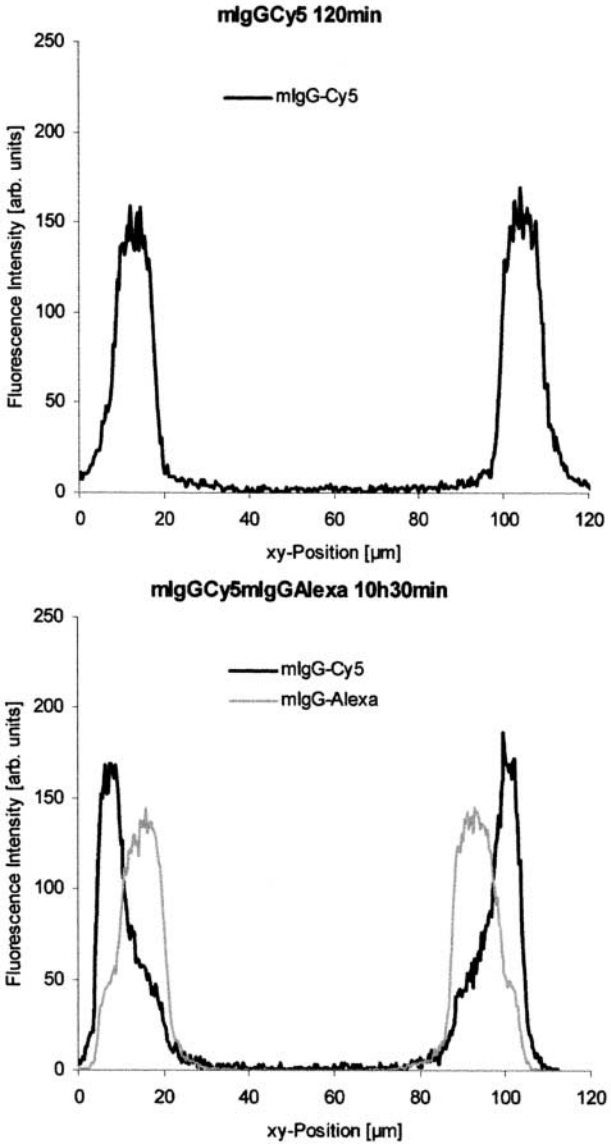

Figure 8. Fluorescence intensity profiles of a sequential incubation of fluorescence labeled mIgG at pH 4.5 with SP Sepharose FF; 50 m*M* acetate buffer (0–120 min mIgGCy5; 2 hr–8 hr 30 min mIgGAlexa; 8 hr 30 min–18 hr mIgG–Cy3).

MARCEL DEKKER, INC.
270 Madison Avenue, New York, New York 10016

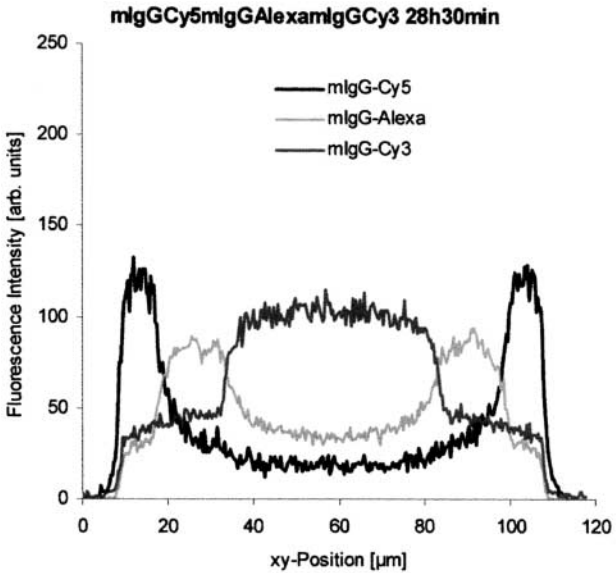

Figure 8. Continued.

be more distributed over the particle diameter than in the case of low conductivity and therefore, are not as consistent with the simple picture of the shrinking core model. It is evident that a change in fluid phase conditions can change the mobility of bound adsorbate molecules within porous stationary phases and thus influence the pattern of protein uptake.

In a second set of experiments, the adsorption of a mouse monoclonal antibody of the subclass 2A (mIgG) to SP Sepharose FF was investigated in 50 m*M* acetate buffer at pH 4.5 and 5.0. Figure 8 shows the fluorescence intensity profiles of the sequential incubation scheme outlined in Fig. 2 at pH 4.5. The initial incubation was performed with a mIgG–Cy5 conjugate for 120 min, the resulting fluorescence response signal is represented by the black line in the first plot. The mIgG penetrates into the adsorbent particles to a depth of approximately 20 μm. Incubation of the pre-loaded particles with a mIgG–Alexa conjugate for 8.5 hr does not change the position of the initially bound mIgG molecules significantly, the second conjugate is transported and bound to regions further inside the stationary phase while the initially bound protein molecules more or less remain in the original binding spots. During further incubation of the particles with an mIgG–Cy3 conjugate for another 18 hr the core of the stationary phase fills up with protein while the already bound molecules do not change position. The resulting equilibrium distribution of conjugates is similar to the

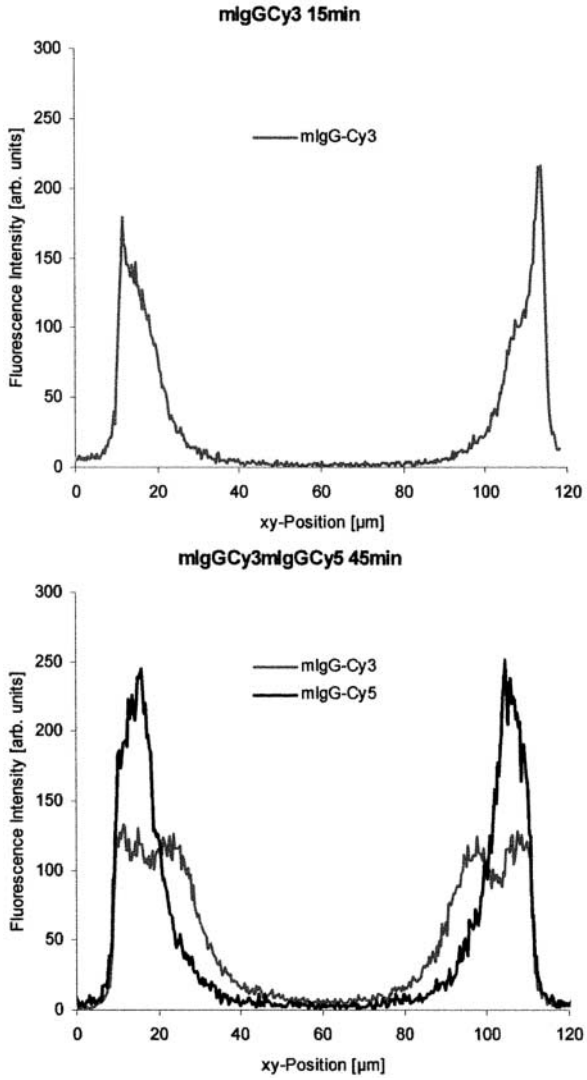

Figure 9. Fluorescence intensity profiles of a sequential incubation of fluorescence labeled mIgG at pH 5.0 with SP Sepharose FF; 50 m*M* acetate (0–15 min mIgGCy3; 15–30 min mIgGCy5; 30 min–25 hr 15 min mIgG–Alexa).

MARCEL DEKKER, INC.
270 Madison Avenue, New York, New York 10016

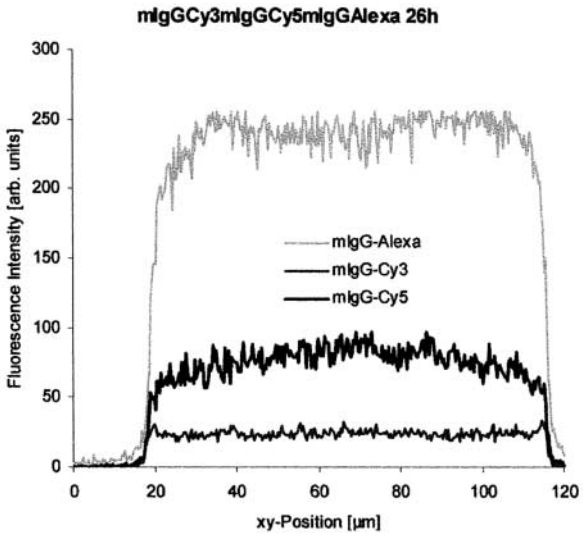

Figure 9. Continued.

situation obtained with BSA at low conductivity and fits the shrinking core model nicely, which describes the gradual 'shell by shell' saturation of a spherical adsorbent particles. In the respective confocal image (not shown), three clearly separated rings of fluorescence can be seen as it is the case with BSA in Fig. 4. The situation drastically changes when the experiment is repeated at pH 5.0 (Fig. 9). Initial incubation with mIgG–Cy3 (grey line) for only 15 min results in penetration of the stationary phase to 30 μm depth, which indicates a significantly faster transport process into the particle. During incubation with the second conjugate (mIgG–Cy5, black line) for 30 min, the conjugate is bound to the external regions of the particle while the initially bound mIgG–Cy3 molecules are further transported towards the core. Incubation with the third conjugate (mIgG–Alexa, light grey line) to equilibrium leads to a situation, where all protein–dye conjugates are evenly distributed within the adsorbent. Similar to the case of BSA, at increased ionic strength a change in mobile phase conditions—in this case a change of pH as opposed to a change in conductivity—leads to a switch in protein uptake pattern from a situation which appears to be consistent with the physical picture of the shrinking core model to a scenario, where protein molecules are transported further towards the particle core subsequent to binding to the outer regions of the adsorbent. In the case of mIgG this strong increase in the overall uptake velocity leads to a drastic change of the uptake pattern in a way that the transport of protein molecules after initial binding is more or less the dominating process. The overall influx seems to be increased by an 'additional'

transport of molecules into the particle, whereas in the case of BSA, the overall influx was similar. One possible explanation of this striking discrepancy may be found in the size of the adsorbate molecules. In the shrinking core model, the adsorbent is filled up from the outside to the inside, thus adsorbate molecules coming in later are transported within the pore fluid and have to pass the already loaded regions, where the presence of bound molecules may lead to narrowed pores and thus to a reduced effective mobility of the moving species. As the molecular weight of the mIgG (ca. 150000 g/mol) is more than double that of BSA (ca. 67000 g/mol), it is not unlikely that this 'narrowing' of available pore space is more significant in case of the larger molecule. If the change in mobile phase conditions leads to a new pattern of protein influx, which allows the movement of bound molecules to the core, newly incoming molecules can bind to the ligands at the rim of the adsorbent and do not have to be transported through 'crowded' pores. Overall, the net rate of influx thus could be increased, as in the case of mIgG at pH 5.0. For BSA, the net gain may not be as impressive because the smaller molecule leads to less blocked pore space and less hindered influx into the core even in the case of a 'shrinking core' transport pattern.

In order to ensure that the uptake patterns were not biased by the fact that differently labeled proteins were used, the fluorescence intensities from the individual protein–dye conjugates were added and compared to the control experiment, where only one protein–dye conjugate had been used in the three incubation periods. As each fluorescent dye has an individual intensity yield after fluorescence excitation, a calibration of the detectors was performed as described in the materials and methods section (see Fig. 3). Figure 10 shows a comparison of the summarized intensity distribution (dotted line) and the control experiment (solid line) in the example of BSA incubation with SP Sepharose FF in 150 m*M* acetate buffer at pH 5.0. As both of the fluorescence profiles are very similar, particular dye related effects can be excluded.

In order to translate the fluorescence intensity profiles into true protein concentration profiles, the absolute protein capacities Q_{abs} were determined for all experiments on the basis of fluid phase protein concentrations, according to Eq. (4). A plot of Q_{abs} vs. the relative capacity Q_{rel} (as calculated from the fluorescence signals after Eqs. (1)–(3)) can be used for calibration, provided a linear behavior is found. This was performed for both protein systems under different fluid phase conditions for all protein–dye combinations. The combined results are shown in Fig. 11A (BSA) and B (mIgG) and they clearly demonstrate that the fluorescence response can be translated into a true protein capacity of the stationary phase with reasonable accuracy. Deviations shown by the error bars in Fig. 11 are predominantly caused by the relatively small volumes to be handled using this method. But these deviations do not blur the qualitative information on transport mechanisms obtained using this approach.

MARCEL DEKKER, INC.
270 Madison Avenue, New York, New York 10016

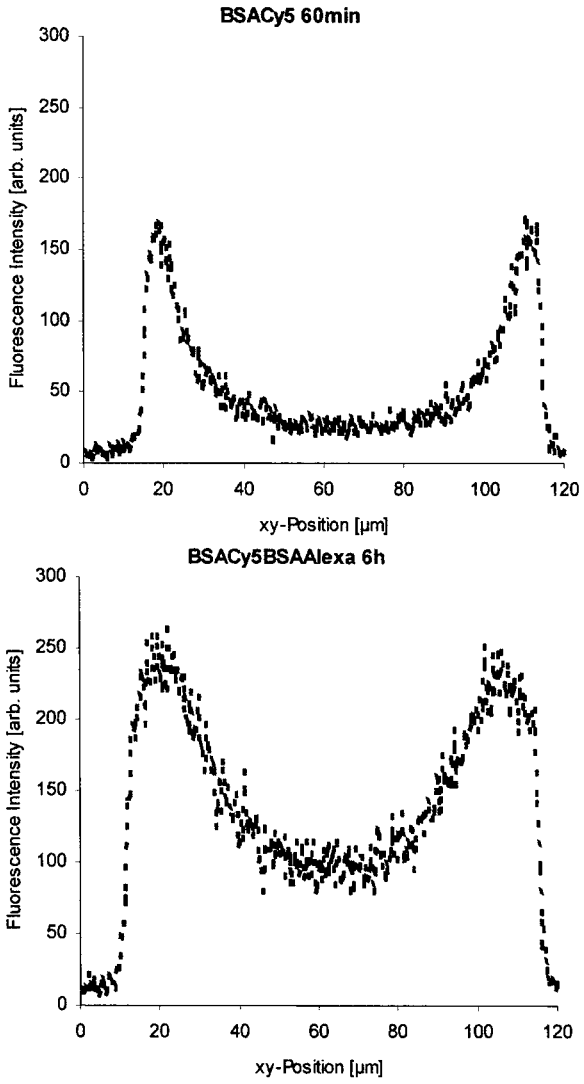

Figure 10. Summarized intensity distribution (dotted line) and single conjugate control experiment (solid line) of BSA incubation with SP Sepharose FF in 150 m*M* acetate buffer at pH 5.0.

(continued)

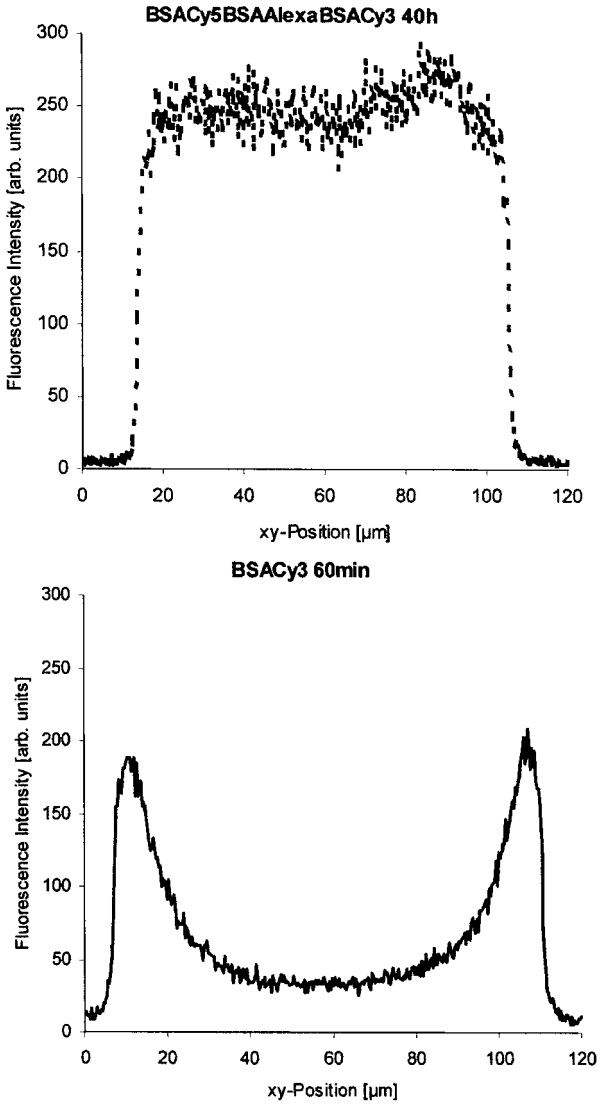

Figure 10. Continued.

MARCEL DEKKER, INC.
270 Madison Avenue, New York, New York 10016

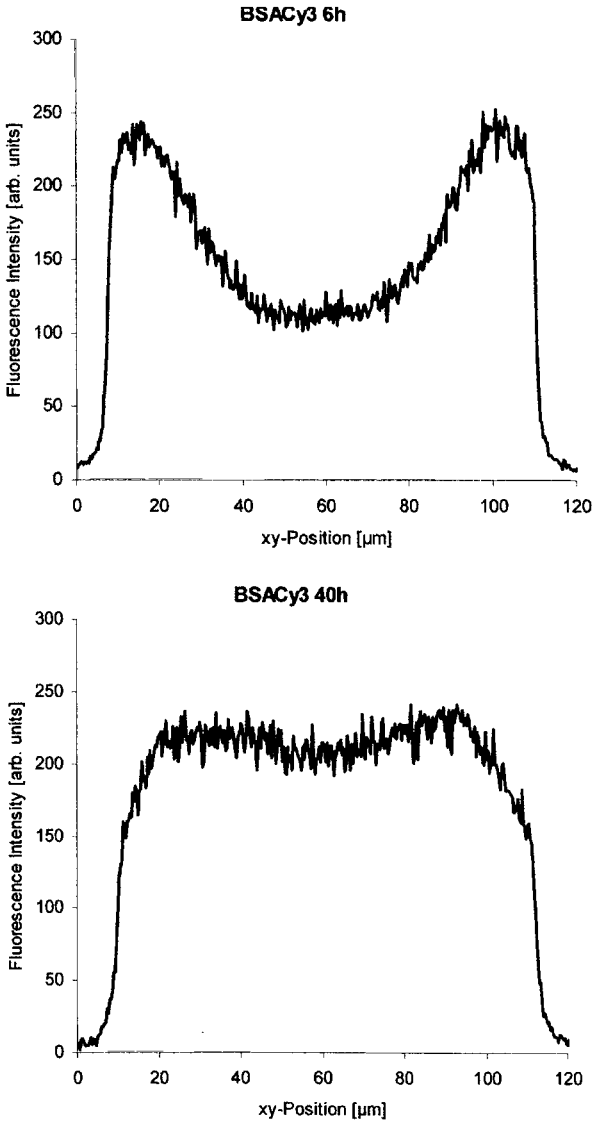

Figure 10. Continued.

MARCEL DEKKER, INC.
270 Madison Avenue, New York, New York 10016

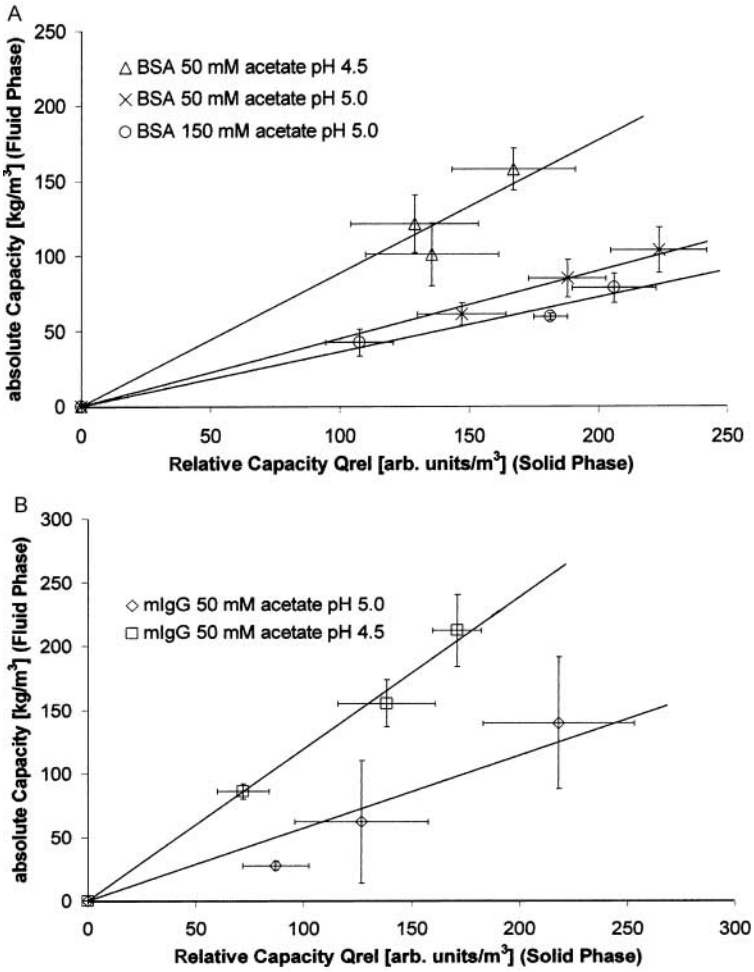

Figure 11. Relative capacity Q_{rel} vs. absolute capacity Q_{abs} for (A) BSA and (B) mIgG adsorption to SP Sepharose FF under different operating conditions.

Adsorption Isotherms

The apparent dependence of the protein uptake pattern on pH and conductivity suggests a correlation to the adsorption equilibrium, which of course is also a function of mobile phase conditions. In order to test this assumption, equilibrium isotherms were generated for both proteins under all investigated conditions. All systems could be described by the Langmuir model (Eq. (5)) and

Table 2. Langmuir Parameters of the Equilibrium Isotherms of all Systems Under Investigation

System	Q_{max} (kg/m^3)	K_a (m^3/kg)
BSA, 50 m*M* acetate pH 4.5	180	25
BSA, 50 m*M* acetate pH 5.0	145	12.5
BSA, 150 m*M* acetate pH 4.5	89	0.9
mIgG, 50 m*M* acetate pH 4.5	226	0.9
mIgG, 50 m*M* acetate pH 5.0	146	5.6

the parameters Q_{max} and K_a could be determined with high accuracy by non-linear fit of the model to the experimental data. Table 2 summarizes the results obtained. In case of BSA, they follow straightforward expectations: an increase in pH reduces the number of positive charges on the protein surface and thus the number of potential interaction sites with the stationary phase, a fact which is mirrored by the reduced maximum binding capacity Q_{max} and the slight reduction in association equilibrium constant K_a. Increased ionic strength in the mobile phase shields the surface charges and therefore has similar consequences for the equilibrium parameters, the overall effect on K_a being more pronounced, however. In the particular case of BSA this means a drastic shift from almost irreversible (low ionic strength) to only moderately favorable equilibrium (increased ionic strength). In case of the monoclonal antibody, the findings are not as straightforward: increasing the pH leads to the expected reduction of Q_{max}, the K_a value, however, is significantly increased, thus shifting the equilibrium from close to linear to almost rectangular. On the basis of the data on BSA adsorption, the 'shrinking core' type uptake pattern at low ionic strength appears to be correlated to an irreversible or very favorable isotherm, which is one of the pre-conditions of the shrinking core model. Less favorable isotherms would then lead to a shift in uptake pattern with an increased mobility of bound molecules. The data on mIgG adsorption, however, seem to contradict this interpretation. Experiments with other proteins and a wider variety of operating conditions will be conducted in order to investigate this phenomenon further.

CONCLUSIONS

In this study we introduced a new experimental technique to investigate in situ different patterns of protein uptake to porous media by visualizing the transport of protein–dye conjugates within adsorbent particles using confocal microscopy. A thorough characterization of the different conjugates in terms of

MARCEL DEKKER, INC.
270 Madison Avenue, New York, New York 10016

biochemical and chromatographic properties indicates that the labeled molecules retain the dominant properties of the unmodified protein and that the results obtained therefore are not biased by the labeling procedure.

In order to develop, optimize, and validate the technique, BSA and a monoclonal IgG2A antibody were chosen as model proteins and adsorbed to the cation exchanger SP Sepharose FF. In the case of BSA, the adsorption pattern seems not to be significantly influenced by the pH in the investigated range (pH 4.5–5.0), although the proteins' isoelectric point of 4.8 suggests a change in net charge within this range. In both cases a behavior very similar to the shrinking core model is found, which predicts a gradual loading of spherical particles from the outside to the inside. The model assumes that the adsorbate is transported in the pore fluid till the fist available ligand and stays in place until the particle is in equilibrium with the fluid phase. This shrinking core pattern is visualized nicely using the three-conjugate approach. Increasing the conductivity in the mobile phase significantly changes the uptake pattern in a way that the mobility of the bound species seems to be increased, which allows molecules to travel further inside the particle and make room for binding of additional molecules at the particle rim. The three-conjugate approach again nicely visualizes this by showing the overlap of protein zones during sequential incubation. As the shrinking core model is only valid for very favorable equilibrium situations, it is reasonable to assume that a deviation from the shrinking core pattern is caused by a change in the binding equilibrium. A determination of the equilibrium isotherms under the different fluid phase conditions shows that in fact a change in pH does not influence the shape of the equilibrium isotherm, which is almost rectangular in both cases. The increase in conductivity, however, results in a shift towards an only moderately favorable isotherm, a fact which supports the above hypothesis. Experiments with mIgG, however, delivered contradictory results: a change in pH resulted in a drastic shift in uptake pattern from pure shrinking core behavior to a situation in which the bound molecules appeared to be extremely mobile. The isotherms, however, were almost linear in the case of the shrinking core pattern and very favorable in the other case, so that no correlation between equilibrium and uptake pattern can be observed at this point.

The technique provided here can be a very valuable tool for further evaluation of the various uptake patterns during protein adsorption to porous particles, which have been discussed extensively in literature on the basis of fluid phase data only (7,8,10,14). This method can give further insight as a translation of the confocal images into particle side protein profiles allows the direct calculation of the relative protein concentration in the adsorbent (capacity). This quantity can be re-calculated into a true capacity in mg of protein per mL of adsorbent by a calibration plot. This gives access to the development of the protein concentration profile with incubation time, which can be compared to

MARCEL DEKKER, INC.
270 Madison Avenue, New York, New York 10016

simulations in order to check the validity of models like, e.g., the shrinking core model or other constructs, which allow a mixed type of influx.

NOMENCLATURE

c_{eq}	protein concentration at equilibrium (kg/m^3)
c_i	initial protein concentration (kg/m^3)
c_t	protein concentration at the time t (kg/m^3)
$I_{integr.}$	integral intensity of fluorescence profile (arbitrary units)
$I_{integr.}^{shell}$	shell volume intensity (arbitrary units)
I_{rad}	fluorescence intensity within a segment (arbitrary units)
K_{av}	coefficient of available volume (distribution coefficient)
K_a	association equilibrium constant (m^3/kg)
Q	capacity (kg/m^3)
Q_{max}	maximum capacity (kg/m^3)
Q_{rel}^{ch}	relative capacity of the fluorescent signal of one channel (kg/m^3)
Q_{rel}	relative capacity (arbitrary units/m^3)
Q_{abs}	absolute capacity (kg/m^3)
r_a	outer radius of particle shell (m)
r_i	inner radius of particle shell (m)
r_p	particle radius (m)
t	time
V_{gel}	gel volume (m^3)
V_P	particle volume (m^3)
V_{sys}	volume of the system (m^3)

ACKNOWLEDGMENTS

The authors are grateful to Barbara Jantsch and Markus Halfar for excellent assistance during the experimental work and to Dr Karol Lacki for making the micro-method for measuring adsorption isotherms available.

REFERENCES

1. Johnson, E.M.; Berk, D.A.; Jain, R.K.; Deen, W.M. Diffusion and Partitioning of Proteins in Charged Agarose Gels. Biophys. J. **1995**, *68*, 1561–1568.
2. Mattisson, C. Diffusion Studies in Gels Using Holographic Laser Interferometry Ph.D. thesis, Lund University **1999**.

MARCEL DEKKER, INC.
270 Madison Avenue, New York, New York 10016

3. Lewus, R.K.; Carta, G. Protein Diffusion in Charged Polyacryamide Gels: Visualisation and Analysis. J. Chromatogr., A **1999**, *865*, 155–168.
4. Ljunglöf, A.; Hjorth, R. Confocal Microscopy as a Tool for Studying Protein Adsorption to Chromatographic Matrices. J. Chromatogr., A **1996**, *743*, 75–83.
5. Ljunglöf, A.; Thömmes, J. Visualising Intraparticle Protein Transport in Porous Adsorbents by Confocal Microscopy. J. Chromatogr., A **1998**, *813*, 387–395.
6. Linden, T.; Ljunglöf, A.; Kula, M.-R.; Thömmes, J. Visualising Two Component Protein Diffusion in Porous Adsorbents by Confocal Scanning Laser Microscopy. Biotechnol. Bioeng. **1999**, *65*, 622–630.
7. Fernandez, M.A.; Carta, G. Characterization of Protein Adsorption by Composite Silica–Polyacryaminde Gel Anion Exchangers I Equilibrium in Agitated Contactors. J. Chromatogr., A **1996**, *746*, 169–183.
8. Fernandez, M.A.; Carta, G. Characterization of Protein Adsorption by Composite Silica–Polyacryaminde Gel Anion Exchangers II. Mass Transfer in Packed Columns and Predictability of Breakthrough Behaviour. J. Chromatogr., A **1996**, *746*, 185–198.
9. Hansen, E.; Mollerup, J. Application of the Two-film Theory to the Determination of Mass Transfer Coefficients for Bovine Serum Albumin on Anion-Exchange Columns. J. Chromatogr., A **1998**, *827*, 259–267.
10. Ma, Z.; Whitley, R.D.; Wang, N.-H.L. Pore and Surface Diffusion in Multicomponent Adsorption and Liquid Chromatography Systems. AIChE J. **1996**, *42* (5), 1244–1262.
11. Weaver, L.E.; Carta, G. Protein Adsorption on Cation Exchangers: Comparison of Macroporous and Gel-Composite Media. Biotechnol. Prog. **1996**, *12*, 342–355.
12. Pawley, J.B. *Handbook of Biological Confocal Microscopy*; Plenum Press: New York, 1995.
13. Ruthven, D.M. *Principles of Adsorption and Adsorption Processes*; Wiley–Interscience: New York, 1984.
14. Tsou, H.-S.; Graham, E.E. Prediction of Adsorption and Desorption of Protein an Dextran-Based Ion-Exchange Resin. AIChE J. **1985**, *31* (12), 1959–1966.

Received September 2000
Revised April 2001

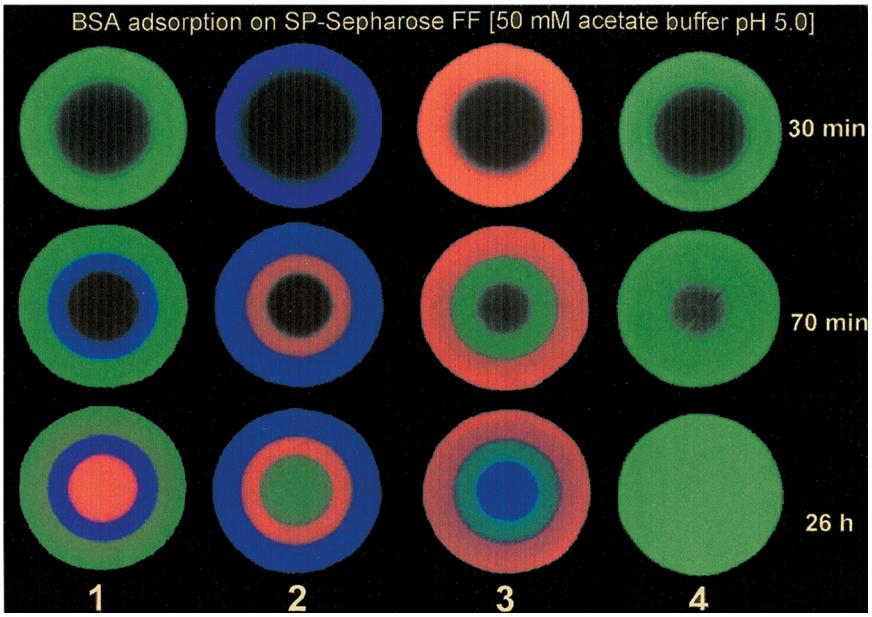

Figure 4. Confocal images of a sequential incubation of different BSA protein/dye conjugates (left three columns of images) and one single conjugate control experiment.

MARCEL DEKKER, INC.
270 Madison Avenue, New York, New York 10016

Request Permission or Order Reprints Instantly!